Fluoride Inhibition of Enolase: Crystal Structure and Thermodynamics[†,‡]

Jie Qin,[§] Geqing Chai,[§] John M. Brewer,[||] Leslie L. Lovelace,[§] and Lukasz Lebioda*[,§,⊥]

Department of Chemistry and Biochemistry and Center for Colon Cancer Research, University of South Carolina, Columbia, South Carolina 29208, and Department of Biochemistry and Molecular Biology, University of Georgia, Athens, Georgia 30602

Received August 4, 2005; Revised Manuscript Received November 16, 2005

ABSTRACT: Enolase is a dimeric metal-activated metalloenzyme which uses two magnesium ions per subunit: the strongly bound conformational ion and the catalytic ion that binds to the enzyme−substrate complex inducing catalysis. The crystal structure of the human neuronal enolase−$Mg_2F_2P_i$ complex (enolase fluoride/phosphate inhibitory complex, EFPIC) determined at 1.36 Å resolution shows that the combination of anions effectively mimics an intermediate state in catalysis. The phosphate ion binds in the same site as the phosphate group of the substrate/product, 2-phospho-D-glycerate/phosphoenolpyruvate, and induces binding of the catalytic Mg^{2+} ion. One fluoride ion bridges the structural and catalytic magnesium ions while the other interacts with the structural magnesium ion and the ammonio groups of Lys 342 and Lys 393. These fluoride ion positions correspond closely to the positions of the oxygen atoms of the substrate's carboxylate moiety. To relate structural changes resulting from fluoride, phosphate, and magnesium ions binding to those that are induced by phosphate and magnesium ions alone, we also determined the structure of the human neuronal enolase−Mg_2P_i complex (enolase phosphate inhibitory complex, EPIC) at 1.92 Å resolution. It shows the closed conformation in one subunit and a mixture of open and semiclosed conformations in the other. The EPFIC dimer is essentially symmetric while the EPIC dimer is asymmetric. Isothermal titration calorimetry data confirmed binding of four fluoride ions per dimer and yielded K_b values of $7.5 \times 10^5 \pm 1.3 \times 10^5$, $1.2 \times 10^5 \pm 0.2 \times 10^5$, $8.6 \times 10^4 \pm 1.6 \times 10^4$, and $1.6 \times 10^4 \pm 0.7 \times 10^4$ M^{-1}. The different binding constants indicate negative cooperativity between the subunits; the asymmetry of EPIC supports such an interpretation.

It has long been known that fluoride ions inhibit alcoholic fermentation and glycolysis. Warburg and Christian have shown that this is due to the inhibition of enolase (*1*). Enolase (2-phospho-D-glycerate hydrolyase, EC 4.2.1.11) is an enzyme functioning in the Embden−Meyerhof−Parnas glycolytic pathway that catalyzes the reversible dehydration of 2-phospho-D-glycerate (PGA)[1] to yield PEP.[1] The enzyme molecule is composed of two identical subunits (*2*) and has a requirement for two divalent cations per active site for catalytic activity. The first one is often referred to as the "conformational" ion because its binding induces a conformational change. The second ion binds only in the presence of a substrate (or its analogues) and is necessary for enzymatic activity. We refer to it as the "catalytic" ion. These cations are Mg^{2+} under physiological conditions but can be replaced by a variety of metal ions (*3*).

The enolase subunit has been found to exist in three major conformational states. The closed conformation has been observed in the catalytic complex with PGA (*4*, *5*) and with strong inhibitors such as phosphonoacetohydroxamate (*6*). The semiclosed conformation has been found in the catalytic complex with PEP (*4*); it differs from the closed conformation in the position of the loop containing His 157, which does not form a direct hydrogen bond with the phosphate moiety but interacts via a water molecule. The open conformation is observed in the absence of substrates or their inhibitory analogues (*7*).

In addition to its significance for the brewing industry, the fluoride inhibition of enolase has practical ramifications in the treatment of dental plaque in which deep layers are highly anaerobic and dependent on glycolysis for energy requirements and, even more importantly, on the presence of PEP for the transport of sugar by the PEP-dependent phosphotransferase system (*8*).

From the very beginning, it was suggested that the inhibition of enolase is due to the formation of a magnesium−fluoride−phosphate complex (*1*). Later, it was found that

[†] This work was supported in part by NIH Grant CA076560. Data were collected at the Southeast Regional Collaborative Access Team (SER-CAT) 22-BM beamline at the Advanced Photon Source, Argonne National Laboratory. Supporting institutions may be found at www.ser-cat.org/members.html. Use of the Advanced Photon Source was supported by the U.S. Department of Energy, Office of Basic Energy Sciences, under Contract W-31-109-Eng-38.

[‡] Atomic coordinates have been deposited with the Protein Data Bank as entries 2AKZ and 2AKM for the structure of the fluoride/phosphate complex and the phosphate complex, respectively.

* Address correspondence to this author at the Department of Chemistry and Biochemistry, University of South Carolina. Phone: (803) 777-2140. Fax: (803) 777-9521. E-mail: lebioda@mail.chem.sc.edu.

[§] Department of Chemistry and Biochemistry, University of South Carolina.

[||] Department of Biochemistry and Molecular Biology, University of Georgia.

[⊥] Center for Colon Cancer Research, University of South Carolina.

[1] Abbreviations: PGA, 2-phospho-D-glycerate; PEP, phosphoenolpyruvate; hNSE, human neuron-specific enolase; EFPIC, enolase fluoride/phosphate inhibitory complex, $(hNSE{\cdot}Mg_2{\cdot}F_2{\cdot}P_i)_2$; EPIC, enolase phosphate inhibitory complex; PDB, Protein Data Bank.

10.1021/bi051558s CCC: $33.50
Published on Web 12/22/2005

rabbit muscle enolase was only weakly affected by F^- alone and that in the presence of P_i the inhibition was strong and competitive with respect to the substrate (*9*). These findings were confirmed by studies (*10*) that showed cooperativity of P_i and F^- binding and, more specifically, that F^- is coordinated to the enzyme-bound Mg^{2+}.

A more detailed study of fluoride binding by yeast enolase was carried out with a fluoride ion-specific electrode by Bunick and Kashket (*11*). They presented evidence for a binding mechanism in which one F^- ion was bound per subunit containing conformational Mg^{2+} ion and P_i. An additional F^- could bind only after additional, presumably catalytic, Mg^{2+} ion bound. The reported dissociation constants for these fluoride ions were 5.0×10^{-4} and 8.2×10^{-5}, respectively. Addition of the substrate, PGA, led to the release of both bound F^- ions in a competitive fashion. However, subsequent studies showed that, in the presence of PGA, yeast enolase is inhibited by F^-, though in a complicated, time-dependent fashion (*12*), becoming noncompetitive over time (cf. ref *10*).

There is a large variation in the strength of F^- inhibition in the presence of different activating cations (*10*, *13*). The Mg^{2+}-activated yeast enzyme is the most strongly inhibited, the Mn^{2+}-activated enzyme is inhibited 40 times more weakly, and the Zn^{2+}-activated enzyme shows no inhibition by F^-. Mn^{2+} ion is, however, paramagnetic and enabled utilization of techniques that are not applicable to Mg^{2+} complexes (*13*, *14*). These studies quantitatively demonstrated strong positive cooperativity in F^- and P_i binding with a 10^2-fold increase in K_d for F^- dissociation from the ternary complex yeast enolase$-Mn^{2+}-F^-$ and a 10^3-fold increase in K_d for P_i dissociation from the enolase$-Mn^{2+}-P_i$ complex when compared to the quaternary complex. The data also indicated that one F^- binds in the active site displacing a water molecule from the first coordination sphere of the bound Mn^{2+} ion. To explain the potency of the inhibition, Nowak and Maurer suggested that the quaternary complex formation induces a transition state-like conformation of the enzyme (*14*).

Zhang et al. reported crystallographic studies of the yeast enolase$-$fluoride$-$phosphate complex (*15*). However, these studies were carried out at a high ammonium sulfate (ca. 2 M) concentration, which prohibited binding of the catalytic magnesium ion and presumably the second fluoride ion. Here we report a higher resolution study of the structure of human neuron-specific enolase in the presence of fluoride, phosphate, and magnesium ions at lower (ca. 0.4 M) ionic strength.

Most of the previous studies were carried out using yeast enolase 1 while here investigations of hNSE are reported to take advantage of the superior scattering power of its crystals. It is likely, however, that the results are applicable also to the yeast enzyme and vice versa since enolase, like all glycolytic enzymes, is strongly conserved. Yeast enolase 1 and NSE are 62% identical (73% similar), with two small (two and one residue) deletions present in all known mammalian enolases. All active site residues are conserved (*16*), and the kinetic parameters are similar (J. M. Brewer and R. Kendrick, unpublished observations).

Inspection of the active site revealed a number of features that are in excellent agreement with previously published solution binding studies (*1*, *9*$-$*14*). The structures reported here likely represent the inhibitory complexes formed at physiological conditions. The fluoride/phosphate binding is confirmed by our isothermal titration calorimetry (ITC) study, which is to our knowledge the first thermodynamic documentation of cooperativity between enolase subunits.

MATERIALS AND METHODS

Crystallography. Recombinant human neuron-specific enolase (hNSE) was expressed in *Escherichia coli*, purified, and crystallized as previously described (*17*). Briefly, crystals were grown from about 20% PEG 4000 solutions, 200 mM $MgCl_2$, and 0.1 M Tris-HCl buffer at pH 8.5. These crystals are large plates, typically $0.5 \times 0.3 \times 0.05$ mm. A crystal was transferred to a cryosolution, which contained 1 mM Mg^{2+} and 2 mM PO_4^{3-}, concentrations that were consistent with the ITC titrations, and 1 mM NaF, 40% PEG 6000, 400 mM KCl, and 15% (w/v) ethylene glycol; the crystal was soaked for 5 min. Another crystal was transferred to a cryosolution, which contained the same components except for 1 mM NaF and was soaked in the same fashion. The crystals were flash frozen in liquid nitrogen and used to collect X-ray diffraction data at the 22BM beamline (SER-CAT) at the Advanced Photon Source in the Argonne National Laboratory. The data were processed with the HKL2000 software (*18*). Mosaicity for both crystals remained low, 0.36° for the hNSE·Mg_2·F_2·P_i complex and 0.41° for the hNSE·Mg_2·P_i complex. The experiment statistics and details are presented in Table 1. The structural model was derived from the native structure (*17*) (PDB entry 1TE6). It was rebuilt with the Turbo-Frodo interactive graphic software (*19*) and refined with the CNS software (*20*) in iterative fashion. Subsequently, the structures were refined using SHELXL (*21*). The EPIC structure was refined using the isotropic approximation for temperature factors. The EFPIC final refinements used the anisotropic approximation and calculated positions for hydrogen atoms (except for the hydroxyls of serine, threonine, and tyrosine residues and for water molecules). The geometry of the final models was verified using PROCHECK (*22*). Protein model superpositions were obtained using the LSQKAB program from the CCP4 package (*23*). Figures 1 and 2 were generated using Turbo-Frodo (*19*). Figure 4 was generated using MOLSCRIPT (*24*) and Raster3D (*25*).

Electrostatics. Calculations of the molecular electrostatic potential were carried out using the DelPhi software (*26*). Models that were used are discussed in the Results section.

Calorimetry. ITC measurements were carried out at 25 °C using a VP-ITC microcalorimeter (Microcal, LLC, Northampton, MA). All solutions were prepared using deionized water. hNSE solution (50 μM) was dialyzed for 24 h against two changes of 1 L of buffer consisting of 10 mM Hepes, pH = 7.6, 1 mM Mg^{2+}, and 2 mM PO_4^{3-}. The second dialysis buffer was saved as stock solution. Fluoride solution (1.63 mM) was prepared by adding solid NaF to the Hepes buffer stock solution, and its pH was carefully adjusted to exactly match the pH of the hNSE solution. Immediately prior to loading the sample cell and the injection syringe, both titrant and sample solutions were thoroughly degassed. Fluoride solution was added, as 4 μL injections, each delivered over 8 s with an interval of 200 s between injections to achieve equilibrium. Titration continued until

Table 1: Crystallographic Data and Refinement Statistics

complex	(hNSE·Mg_2·F_2·P_i)$_2$ EFPIC	(hNSE·Mg_2·P_i)$_2$ EPIC
X-ray source	22BM	22BM
detector	Mar250	Mar250
wavelength (Å)	0.99997	1.00000
temp (K)	100	100
no. of frames	230	159
oscillation range (deg)	0.500	1.000
detector to crystal distance (mm)	120	170
space group	$P2_12_12$	$P2_12_12$
unit cell dimensions		
a (Å)	109.007	111.739
b (Å)	118.515	119.692
c (Å)	67.189	68.299
volume (Å^3)	862317	913458
mosaicity (deg)	0.36	0.41
resolution range (Å) (outer shell)[a]	50.00−1.36 (1.41−1.36)	50.00−1.92 (1.99−1.92)
average *I*	6684.5	725.0
average $I/\sigma(I)$	12.5	6.3
no. of unique reflections	163485 (9249)	56605 (2766)
redundancy	4.1 (1.6)	3.1 (2.1)
completeness (%)	88.3 (50.5)	80.2 (39.7)
low-resolution linear *R*-factor (Å) (in shell)	0.034 (50.0−2.93)	0.056 (50.0−4.14)
total linear R_{merge}[b]	0.070 (0.349)	0.097 (0.432)
rejections in merging (%)	0.09	1.7
square R_{merge}	0.048 (0.312)	0.075 (0.428)
no. of reflections with $\lvert F\rvert/\sigma\lvert F\rvert > 2$ in SHELX refinements	150984	43148
R-value[c]	19.02 {11.18}	21.14
R_{free} (5.0% of reflection)[d]	20.57 {14.43}	24.92
rmsd, bond lengths (Å)	0.005	0.006
rmsd, bond angles (deg)	1.3	1.2
average *B*-factor (Å^2)		
for subunit A	16.2	35.8
for subunit B	15.2	33.0
for solvent	22.9	36.4
for Mg^{2+}	9.5	35.8
for F^-	12.2	no F^-
Ramachandran statistics[e]		
residues most favored, ϕ/ψ (%)	89.1	85.0
residues in additionally allowed region (%)	10.6	14.5
contents of asymmetric unit		
amino acid residues	868	866
no. of water molecules	478 {972}	369
ions	4Mg^{2+}, 2PO_4^{3-}, 4F^-, 1Tris	3Mg^{2+}, 2PO_4^{3-}, 1Tris

[a] Values in parentheses are for the outermost resolution shell; values in braces are for the SHELX refinements. [b] $R_{merge} = (\sum_h|I_h - \langle I\rangle|)/(\sum_h I_h)$. [c] $R = (\sum_h|F_o - F_c|)/(\sum_h F_o)$. [d] R_{free} = crystallographic *R*-factor for the test set as implemented in CNS (*20*). [e] Determined with PROCHECK (*22*).

no fluoride solution was left in the syringe; a total of 41 injections were conducted. Prior to the measurement, water−water and buffer−buffer titrations were performed to make sure the instrument worked properly. In addition, a background titration, consisting of the identical titrant solution but with only the buffer solution in the sample cell, was carried out at the beginning of the experiment. The whole ITC experiment was done using standard operational parameters suggested in the MicroCal VP-ITC user manual. The best fit was obtained using the ORIGIN software provided by the manufacturer.

RESULTS

Quality of the Model. Since the data reported here for EFPIC are of significantly higher resolution than those for any other enolase structure, the model was carefully inspected and revised if necessary, including partial occupancy for some side chains. There is excellent electron density for most of the structure; a representative sample is shown in Figure 1. Missing density for the peptide chain is only for residues 434−439 of the C-terminal His tag. The model of EPIC is of lower quality; it appears that a significant fraction of the molecules in subunit B are in the open and the semiclosed conformations. The occupancy of the open conformation is clearly lower than that of the main conformer and was not included in the refined model.

Ligand Presence. Previous binding studies (*11*) indicated that fluoride binds in the active site, since inhibition is competitive, and upon substrate binding both F^- ions bound to the enolase subunit are released. This finding is supported by our studies since the overall structure of the inhibitory complex very closely resembles that of the native enzyme and shows no evidence of onset of unfolding. Also, the subunit interface is very similar, indicating that a disruption of the enolase dimer does not take place; inhibition of human enolase α (*27*) and yeast enolase isozyme 1 (*28*) by chloride ions is due to dimer dissociation. Thus, it can be concluded that fluoride/phosphate inhibition of enolase is due to the active site occupation.

Inspection of the active site revealed a number of features that are in excellent agreement with previously published solution binding studies (*1*, *7*−*9*). Electron density showed a tetrahedral peak in the position corresponding to the phosphate moiety of the substrate which was assigned to the inhibitory phosphate ion. Next to it, there was a strong density, shown in Figure 2, which indicated binding of Mg^{2+} ion in the catalytic ion binding site. It should be noted that the NSE crystals are catalyticaly active and, upon soaking them in artificial mother liquor containing 2-PGA, a complex with bound product, PEP, is observed (Chai et al., unpublished results).

Fluoride Ion Identification. Identification of F^- ions using crystallography is not straightforward since the ions are isoelectronic with water molecules and the expected heights of peaks in electron density maps are very similar. Also, the radii of the fluoride ion (1.36 Å) and the water molecule (1.40 Å) are so similar that they cannot be used alone to identify the ligand. Therefore, the assignment of fluoride ion positions in a protein structure must take into account the environment of solvent peaks and noncrystallographic information. Since the higher affinity F^- binding site with $K_d = 8.2 \times 10^{-5}$ is present only when the catalytic metal ion is available (*11*), it is highly likely that this site is in the coordination sphere of the catalytic Mg^{2+} ion. Its octahedral coordination includes two protein oxygen atoms, O_γ and the carbonyl oxygen of Ser 39, an oxygen atom of the phosphate ion, and three solvent peaks, one of which must correspond to F^- and two to water molecules. Two positions, to which we have assigned water molecules, have environments that are dominated by negatively charged residues and thus are

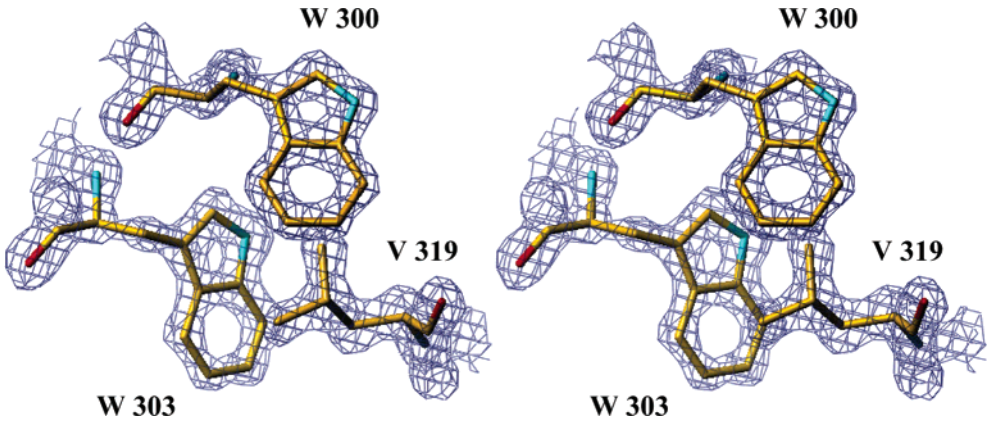

FIGURE 1: Composite omit map ($2F_o - F_c$) of the EFPIC structure at a 2.5σ level.

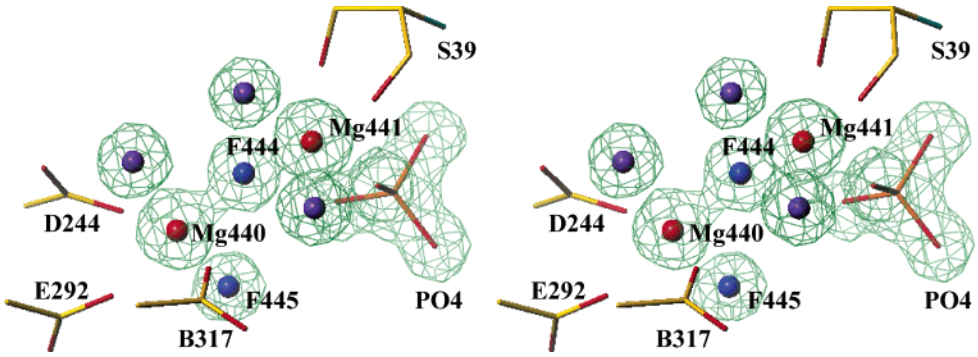

FIGURE 2: Omit electron density map ($F_o - F_c$) in the active site contoured at a 5.0σ level. The Mg ions and water molecules, fluoride ions, and the phosphate ion coordinated to them were omitted from the model.

unsuitable for an anion. Water 447 forms a short contact with Asp 318 (bonding distances are shown in Figure 3) and does not have positively charged neighbors other than the Mg^{2+} ion. Water 448 has contacts with two carboxylates from Asp 317 and Asp 318 and the ammonio group of Lys 342. The third position bridges the two Mg^{2+} ions with suitable distances and a bond angle of 139° (in both subunits). The only negative charges in its environment are those of other atoms coordinated to the metal ions. The bridging ligand functions as an acceptor of a hydrogen bond from Nϵ of Gln 165. This position is much more suitable for fluoride ion binding than the first two, and therefore we assigned to it a fluoride ion, F 444.

The lower affinity F^- binding site with a K_d of 5.0×10^{-4} is present in the absence of the catalytic metal ion (*11*) and thus is located at the conformational metal ion. Inspection of the active site revealed an octahedral coordination of the conformational Mg^{2+} ions with three monodentate carboxylate groups and three solvent (water/fluoride ion) peaks (Figure 2). The peak bridging the two cations has been assigned to the high-affinity fluoride (vide supra) so out of the two peaks remaining, one is a water molecule and the other a fluoride ion. The peaks have very different environments. One peak, to which we assigned water 446, forms contacts with two carboxylates (Asp 244 and Asp 293); the other peak has contacts with two ammonio groups of Lys 342 and Lys 393. This positively charged environment would stabilize an F^- ion binding, and therefore we assigned to it the second fluoride ion, F 445.

This qualitative analysis was confirmed by calculations of molecular electrostatic potential at the positions of waters/fluorides using the DelPhi software. In the first round of calculations all fluoride ions were replaced by water molecules. The highest potentials, which correspond to the most favorable position for negative charges, were in both subunits at site 444, located between the Mg^{2+} ions (Table 2), and the next highest were at position 445. Since the binding of the first fluoride ion affects the molecular electrostatic potential, in the second round of calculations we introduced the negative charge in position 444 by placing a fluoride ion there and repeated the calculations. Site 445 showed the highest potential in both subunits (Table 2). Thus electrostatic considerations unequivocally point to the location of fluoride ions.

Table 2: Electrostatic Potential at Water/Fluoride Binding Sites in kT/e Units

	water molecules only, no F^- ions		F^- ion in position 444	
site	subunit A	subunit B	subunit A	subunit B
444	281	338		
445	206	242	115	152
446	50	55	43	35
447	135	162	48	72
448	158	189	81	108

Although fluoride ion and the water molecule are isoelectronic, their scattering factors at high resolutions are significantly different. At the resolution corresponding to the limit of our data the scattering factors for F^- and O or O^- (as approximations for H_2O) are 4.20, 3.38, or 3.35 electrons, respectively (*29*). We sought confirmation of electrostatics with X-ray diffraction and refined the structure of the complex with fluoride ions in the positions identified by electrostatics or with water molecules. As expected, the *B*-factor values for the waters in positions 444 and 445 were

Table 3: *B*-Factors for Mg^{2+}, F^-, and H_2O (W) in the Active Site of Complex (hNSE·Mg_2·F_2·P_i)$_2$ Obtained in Refinements with F^- or W (H_2O) in Positions 444 and 445[a]

	subunit A	subunit B	subunit A	subunit B
Mg (440)	9.54	8.43	9.92	8.41
Mg (441)	9.28	7.84	9.99	7.63
(444)	F 9.50	F 8.36	W 7.15	W 6.78
(445)	F 14.50	F 14.04	W 12.85	W 12.37
H_2O (446)	11.04	9.60	10.88	9.59
H_2O (447)	10.66	9.74	10.52	8.86
H_2O (448)	10.05	8.12	10.01	8.12

[a] Isotropic approximation and CNS software were used for these tests.

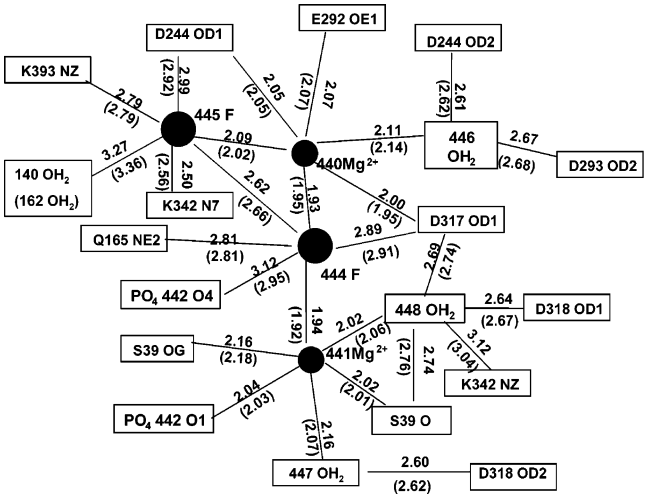

FIGURE 3: Interatomic distances in the active site. The values for subunits A and B (in parentheses) are given.

lower than for fluoride ions (Table 3). Importantly, the *B*-factors for H_2O 444 molecules, the ones bridging the magnesium ions, were significantly smaller than those for Mg^{2+} 440 and Mg^{2+} 441 or other water molecules in the coordination sphere, while for fluoride ion in these positions the *B*-factors were essentially the same. It is not expected that a water molecule bridging two cations would have a *B*-factor lower than the metal ions, so this computational experiment confirms our analysis of electrostatics and supports the presence of fluoride ion in position 444. The temperature factors of fluoride ions 445 are higher than those for the magnesium ions (Table 3), and the same argument cannot be applied. It may be speculated that the higher *B*-factor values of F 445 reflect the presence of some water molecules in this site, which would have their position slightly shifted to form an H-bond with the phosphate ion. Such an interpretation is suggested by difference Fourier maps (not shown).

The Mg^{2+} ions' coordination is summarized in Figure 3. It shows that for the bridging fluoride the distances to the magnesium ions, which are in a 1.92−1.95 Å range, are significantly shorter than to the other ligands. They are in excellent agreement with the values observed in a small molecule compound, catena(trisodium(μ_2-fluoro)(methylenediphosphonate)magesium monohydrate), where a distance of 1.944 Å was observed for a very similar bonding situation (*30*). This distance is also significantly shorter than the analogous distances of 2.12 Å observed in subunit A of the native structure (*17*) where the ligand bridging magnesium ions is a water molecule or hydroxide ion.

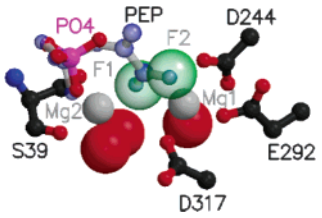

FIGURE 4: Superposition (based on the enzyme C_α atoms) of the yeast enolase−PEP complex (PDB entry 2ONE) on the active site of EFPIC. The proposed positions of fluoride ions (in pale green) overlap with the oxygen atoms of the carboxylate of PEP (in pale blue). Also, there is an excellent correspondence between the positions of the inhibitory phosphate ion (in purple) and the phosphate moiety of PEP. The magnesium ions, Mg1 conformational and Mg2 catalytic, are shown in silver and water molecules in red.

Although the resolution of the diffraction data reported here for EFPIC (1.36 Å) is very high for a protein of the size of enolase, it was insufficient to directly observe the positions of hydrogen atoms in difference Fourier maps.

The ligand assignment proposed above shows that the positions of the fluoride ions correspond to the positions of the carboxylate oxygen atoms of the substrate (Figure 4). This is in agreement with independent data showing the release of both fluoride ions upon substrate binding (*11*). We therefore conclude that the crystals are of the complex (hNSE·Mg_2·F_2·P_i)$_2$, and it is correct to refer to it as the enolase fluoride/phosphate inhibitory complex (EFPIC).

Enolase Phosphate Inhibitory Complex (EPIC). The quality of the data obtained for a crystal soaked in the phosphate solution was somewhat lower. We use this structure to document two findings: First, in the absence of fluoride the conformation of hNSE subunit B is different, and this indicates that the structural differences observed between the native and soaked crystals cannot be attributed to the presence of phosphate alone. Second, the environment of phosphates in the two subunits is different, and this asymmetry propagates to the subunit interface.

Dimer Symmetry. In EFPIC, the dimer is quite symmetric with a rms deviation between the positions of C_α of 0.45 Å. The angle of rotation is 179.6°, indicating almost perfect 2-fold symmetry. In EFPIC in both subunits the active site loop 153−160 is in the closed conformation, and the side chain of His 157 forms a hydrogen bond to the phosphate ion. This is in contrast to the situation found in the native crystals from which the inhibitory complexes presented here were obtained by soaking. The native structure is highly asymmetric; it contains a sulfate (or phosphate) ion and two Mg^{2+} ions in one subunit and a chloride ion and one Mg^{2+} ion in the other (*17*), thus representing a complex hNSE·$2Mg^{2+}$·P_i/hNSE·Mg^{2+}·Cl^-, where "/" separates the subunits. Subunit A (containing sulfate/phosphate) is in the closed conformation, very similar to that observed in both the EFPIC and the EPIC structures reported here, while subunit B is in the open conformation with the position of Ser 39 different by over 11 Å and similar to the EPIC. A least-squares superposition of the native structure and EFPIC complex structure is shown in Figure 5.

The dimer symmetry of the EFPIC complex structure persists at the subunit interface where the side chain of Asn 205 forms two hydrogen bonds with Gly 159 in both subunits. In contrast, in the native structure only hydrogen

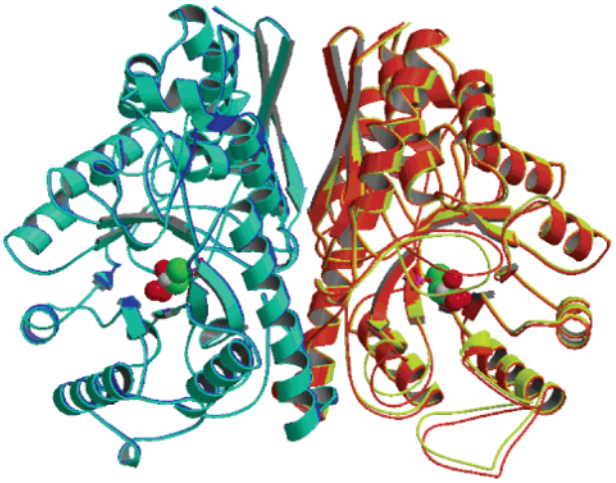

FIGURE 5: Superposition of the EFPIC in cyan (subunit A) and orange (subunit B) and the native (hNSE·$2Mg^{2+}$·P_i/hNSE·Mg^{2+}·Cl^-) complex in blue (subunit A) and yellow (subunit B). The ligands are shown only for the EFPIC structure using the same colors as in Figure 4. It is apparent that subunits A are very similar, but large differences between catalytic loops are present in subunits B.

bonds between Asn 205 B and Gly 159 A are observed. It may be proposed that the tight inhibitory complex resembles the transition state and these additional hydrogen bonds are a part of its stabilization. However, in the absence of inhibitor the dimer is asymmetric, and forces that induce asymmetry by keeping the loops open in subunit B must exist. Consequently, a part of the inhibitor binding energy has to be used to induce the loop closure, and thus binding of the inhibitory ions in subunit B should be weaker.

To verify this hypothesis, the fluoride ion binding constants, K_b, were measured using ITC. K_b values were obtained by fitting the observed heat changes via an iterative process using the Origin 5 software package. The equilibrium binding constants and the binding enthalpy were allowed to vary during the fitting process. The best fit was obtained for a model with four sequential fluoride binding sites. In this model the binding constants are defined relative to the progress of saturation: $K_1 = [EF]/[E][F^-]$; $K_2 = [EF_2]/[EF][F^-]$; ... $K_4 = [EF_3]/[EF_2][F^-]$. The fraction of total macromolecules having n bound ligands is given by $P_n = K_1K_2...K_n[F^-]^n/\{1+K_1[F^-]+K_1K_2[F^-]^2+...+K_1K_2...K_n[F^-]^n\}$, and the heat content after each injection can be calculated from $Q = E_tV_0\{P_1\Delta H_1 + P_2(\Delta H_1 + \Delta H_2) + ... + P_4(\Delta H_1 + \Delta H_2 + \Delta H_3 + \Delta H_4\}$, where E_t is the total enzyme concentration, V_0 is the volume of the calorimeter cell, and ΔH_i are enthalpy changes associated with the binding of sequential fluoride ions. Changes in heat content were used in the Marquardt algorithm to obtain the best values for the eight fitting parameters.

Alternative models in which the four binding sites were constrained to two pairs of equivalent sites (Figure 6), a model used in previous studies (*11*), were inadequate; the values of χ^2 were higher by a factor of 74 or larger. The binding data are summarized in Table 4. They indicate binding of fluoride ions stronger by a factor of 10−20 than reported previously (*11*), but the source of the enzyme (human and yeast) and the buffer used (Hepes and Tris) are different. Asymmetrically bound Tris is observed in both

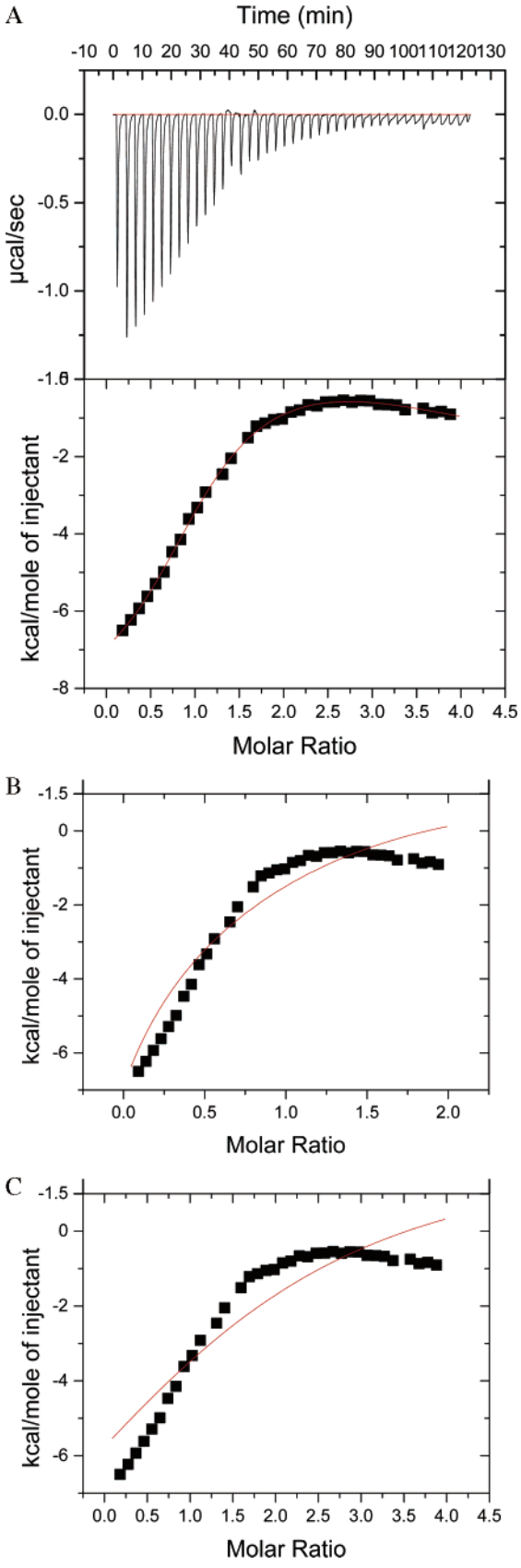

FIGURE 6: Isothermal titration of hNSE with fluoride. (A) The upper panel shows raw data. The lower panel shows the enthalpogram retrieved from these data; the line represents the least-squares fit to a four sequential binding sites model with a χ^2 value of 3.4×10^3. (B) Fit to a two sets of two identical sequential binding sites yielded a χ^2 value of 2.6×10^5. (C) Fit to two independent binding sites, each with a multiplicity of 2, yielded a χ^2 value of 5.6×10^5.

Table 4: Best Fit of the ITC Data for Titration of hNSE with Fluoride to a Model with Four Sequential Binding Sites[a]

	K_b (mol^{-1})	ΔG (kJ mol^{-1})	ΔH (kJ mol^{-1})	$T\Delta S$[b] (kJ mol^{-1})
n_1	$7.5 \times 10^5 \pm 1.3 \times 10^5$	-33.5 ± 0.4	-7.0 ± 0.1	26.5 ± 0.3
n_2	$1.2 \times 10^5 \pm 0.2 \times 10^5$	-29.1 ± 0.4	-1.5 ± 0.5	27.6 ± 0.8
n_3	$8.6 \times 10^4 \pm 1.6 \times 10^4$	-28.1 ± 0.5	2.4 ± 1.0	30.5 ± 1.5
n_4	$1.6 \times 10^4 \pm 0.7 \times 10^4$	-23.6 ± 1.2	-5.9 ± 0.4	17.8 ± 1.0

[a] $\chi^2 = 3547$ (shown in Figure 6). [b] Measured at $T = 298$ K.

EFPIC and EPIC complexes (Table 1) as well as in the native crystals (*17*).

DISCUSSION

Crystallography, electrostatics, and binding data are all consistent with the proposed assignment of the fluoride ions in EFPIC. We are not aware of any data that would not be in agreement with the proposed structure.

The ITC data strongly support the hypothesis of negative cooperativity between subunits for fluoride binding since a set of four K_b is needed to fit the titration curve. Crystallographic studies showing asymmetry of a homooligomeric protein always reflect some correlation of the asymmetry with the crystal packing; otherwise, disorder between the two states would be observed. This leads to the question of whether the asymmetry is not an artifact of the crystal field. The ITC data reported here show that the cooperativity between subunits of hNSE is an intrinsic property of enolase. Subunit cooperativity appears to play a role in enolase catalytic activity. The replacement of Asn 205 (Asn 207 in yeast), a residue central in the dimer asymmetry, with Ala led to reduction of yeast enolase activity by a factor of 5 (*31*), despite the location of this residue far from the active site. Holleman (*32*) showed using "active enzyme centrifugation" that yeast enolase monomers were active (at 40 °C and at hydrostatic pressures approaching 250 atm). Under physiological conditions, enolases are oligomeric (*33*), and there is evidence (refs *5* and *17* and unpublished results) that the subunits interact in terms of ligand binding and catalysis.

Complexes of enolase with strong inhibitors, fluoride/phosphate and phosphonoacetohydroxamate, $K_i = 15$ pM (*6*), which presumably mimic an intermediate state, are symmetric. This suggests that the transition state is also symmetric. On the other hand, a mixed complex with PGA in one subunit and PEP in the other (substrate/product) is asymmetric (*5*). Thus P_i, a weak inhibitor, by itself appears to be a substrate analogue rather than the transition state analogue.

ACKNOWLEDGMENT

We thank Stephen Foundling for help with X-ray data collection at the SER-CAT beamline.

REFERENCES

1. Warburg, O., and Christian, W. (1941) Isolierung und kristallisation des garungsferments enolase, *Biochem. Z. 310*, 384−421.
2. Brewer, J. M., and Weber, G. (1968) The reversible dissociation of yeast enolase, *Proc. Natl. Acad. Sci. U.S.A. 59*, 2l6−223.
3. Brewer, J. M. (1981) Yeast enolase: mechanism of activation by metal ions, *CRC Crit. Rev. Biochem. 11*, 209−254.
4. Larsen, T. M., Wedekind, J. E., Rayment, I., and Reed, G. H. (1996) A carboxylate oxygen of the substrate bridges the magnesium ions at the active site of enolase: structure of the yeast enzyme complexed with the equilibrium mixture of 2-phosphoglycerate and phosphoenolpyruvate at 1.8 Å resolution, *Biochemistry 35*, 4349−4358.
5. Zhang, E., Brewer, J. M., Minor, W., Carreira, L. A., and Lebioda, L. (1997) Mechanism of enolase: the crystal structure of asymmetric dimer enolase-2-phospho-D-glycerate/enolase-phosphoenolpyruvate at 2.0 Å resolution, *Biochemistry 36*, 12526−12534.
6. Wedekind, J. E., Poyner, R. R., Reed, G. H., and Rayment, I. (1994) Chelation of serine 39 to Mg^{2+} latches a gate at the active site of enolase: structure of the bis(Mg^{2+}) complex of yeast enolase and the intermediate analogue phosphonoacetohydroxamate at 2.1-Å resolution, *Biochemistry 33*, 9333−9342.
7. Lebioda, L., Stec, B., and Brewer, J. M. (1989) The structure of yeast enolase at 2.25 Å resolution. An eightfold $\beta\alpha$ barrel with a novel $\beta\beta\alpha\alpha(\beta\alpha)_6$ topology, *J. Biol. Chem. 264*, 3685−3693.
8. Hata, S., Iwami, Y., Kamiyama, K., and Yamada, T. (1990) Biochemical mechanisms of enhanced inhibition of fluoride on the anaerobic sugar metabolism by *Streptococcus sanguis*, *J. Dent. Res. 69*, 1244−1247.
9. Cimasoni, G. (1972) Inhibition of enolase by fluoride in vitro, *Caries Res. 6*, 93−102.
10. Wang, T., and Himoe, A. (1974) Kinetics of the rabbit muscle enolase-catalyzed dehydration of 2-phosphoglycerate, *J. Biol. Chem. 249*, 3895−3902.
11. Bunick, F. J., and Kashket, S. (1982) Binding of fluoride by yeast enolase, *Biochemistry 21*, 4285−4290.
12. Spencer, S. G., and Brewer, J. M. (1982) Substrate-dependent inhibition of yeast enolase by fluoride, *Biochem. Biophys. Res. Commun. 106*, 553−558.
13. Maurer, P. J., and Nowak, T. (1981) Fluoride inhibition of yeast enolase. 1. Formation of the ligand complexes, *Biochemistry 20*, 6894−6900.
14. Nowak, T., and Maurer, P. J. (1981) Fluoride inhibition of yeast enolase. 2. Structural and kinetic properties of the ligand complexes determined by nuclear relaxation rate studies, *Biochemistry 20*, 6901−6911.
15. Lebioda, L., Zhang, E., Lewinski, K., and Brewer, J. M. (1993) Fluoride inhibition of yeast enolase: crystal structure of the enolase-Mg^{2+}-F-P_i complex at 2.6 Å resolution, *Proteins 20*, 219−225.
16. Brewer, J. M., and Lebioda, L. (1997) Current perspectives on the mechanism of catalysis by the enzyme enolase, *Adv. Biophys. Chem. 6*, 111−141.
17. Chai, G., Brewer, J. M., Lovelace, L. L., Aoki, T., Minor, W., and Lebioda, L. (2004) Expression, purification and the 1.8 Å resolution crystal structure of human neuron specific enolase, *J. Mol. Biol. 341*, 1015−1021.
18. Otwinowski, Z., and Minor, W. (1997) Processing of X-ray diffraction data collected in oscillation mode, *Methods Enzymol. 276*, 307−326.
19. Russel, A., and Cambillau, C. (1991) "Turbo Frodo" Silicon Graphics Geometry Partners Directory, p 86, Silicon Graphics, Mountain View, CA.
20. Brunger, A. T., Adams, P. D., Clore, G. M., Delano, W. L., Gros, P., Grosse-Kunstleve, Reed, R. J., Jiang, J., Kuszewskic, J., Nilges, M., Pannu, N., Read, R. J., Rice, L. M., Simonson, T., and Warren, G. L. (1998) Crystallography and NMR system: A new software suite for macromolecular structure determination, *Acta Crystallogr. D54*, 905−921.
21. Sheldrick, G. (1997) http://shelx.uni-ac.gwdg.de/SHELX/.
22. Laskowski, R. A., MacArthur, M. W., Moss, D. S., and Thornton, J. M. (1993) PROCHECK: a program to check the stereochemical quality of protein structures, *J. Appl. Crystallogr. 26*, 283−291.
23. CCP4 (1994) The CCP4 suite: Programs for protein crystallography, *Acta Crystallogr. D50*, 760−763.
24. Kraulis, P. J. (1991) MOLSCRIPT: a program to produce both detailed and schematic plots of protein structures, *J. Appl. Crystallogr. 24*, 946−950.
25. Merritt, E. A., and Bacon, D. J. (1997) Raster3D: photorealistic molecular graphics, *Methods Enzymol. 277*, 505−524.
26. Rocchia, W., Alexov, E., and Honig, B. (2001) Extending the applicability of the nonlinear Poisson−Boltzmann equation: Multiple dielectric constants and multivalent ions, *J. Phys. Chem. B 105*, 6507−6514.
27. Marangos, P. J., and Schmechel, D. E. (1987) Neuron specific enolase, a clinically useful marker for neurons and neuroendocrine cells, *Annu. Rev. Neurosci. 10*, 269−295.

28. Brewer, J. M. (1969) The interaction of potassium chloride and acetate with yeast enolase, *Arch. Biochem. Biophys. 134*, 59−66.
29. *International Tables for X-ray Crystallography* (1974) Vol. 4, p 73, Kynoch Press, Birmingham, England.
30. Dister, A., Lohse, D. L., and Sevov, S. C. (1999) Chains, planes, and tunnels of metal diphosphonates: synthesis, structure, and characterization of $Na_3Co(O_3PCH_2PO_3)(OH)$, $Na_3Mg(O_3PCH_2PO_3)F{\cdot}H_2O$, $Na_2Co(O_3PCH_2PO_3){\cdot}H_2O$, $Na_2Co(O_3PCH_2CH_2CH_2PO_3)(OH)$, and $Co_2(O_3PCH_2PO_3)(H_2O)$, *J. Chem. Soc., Dalton Trans. 1999*, 1805−1812.
31. Brewer, J. M., Glover, C. V. C., Holland, M. J., and Lebioda, L. (2003) Enzymatic function of loop movement in enolase: Preparation and some properties of H159N, H159A, H159F and N207A enolases, *J. Protein Chem. 22*, 353−361.
32. Holleman, W. H. (1973) The use of absorption optics to measure dissociation of yeast enolase into enzymatically active monomers, *Biochim. Biophys. Acta 327*, 176−185.
33. Wold, F. (1971) Enolase, in *The Enzymes* (Boyer, P. D., Ed.) Vol. 5, 3rd ed., pp 499−538, Academic Press, New York.

BI051558S